


Emergence of biconnected clusters in explosive percolation

Liwenying Yang and Ming Li 

School of Physics, Hefei University of Technology, Hefei, Anhui 230009, China



(Received 12 March 2024; accepted 1 July 2024; published 16 July 2024)

By introducing a simple competition mechanism for bond insertion in random graphs, explosive percolation exhibits a sharp phase transition with rich critical phenomena. We investigate high-order connectivity in explosive percolation using an event-based ensemble, focusing on biconnected clusters, where any two sites are connected by at least two independent paths. Our numerical analysis confirms that explosive percolation with different intracluster bond competition rules shares the same percolation threshold and universality, with biconnected clusters percolating simultaneously with simply connected clusters. However, the volume fractal dimension d_f' of biconnected clusters varies depending on the competition rules of intracluster bonds. The size distribution of biconnected clusters exhibits double-scaling behavior: large clusters follow the standard Fisher exponent derived from the hyperscaling relation $\tau' = 1 + 1/d_f'$, while small clusters display a modified Fisher exponent $\tau_0 < \tau'$. These findings provide insights into the intricate nature of connectivity in explosive percolation.

DOI: [10.1103/PhysRevE.110.014122](https://doi.org/10.1103/PhysRevE.110.014122)

I. INTRODUCTION

Explosive percolation (EP), proposed by Achlioptas *et al.* [1], has become a prominent topic in percolation theory and network science [2–4]. The core mechanism of EP is the suppression of large cluster growth when new bonds are inserted, a process known as the Achlioptas process [1]. A typical example is the product rule [1]: starting with a null graph, two potential bonds are chosen at each time step, and the bond that minimizes the product of the sizes of the clusters it connects is inserted, while the other is discarded. This can be generalized to the best-of- m rule or min-cluster- m rule [5], where more than two potential bonds are considered, and various criteria can be used for bond selection [2].

The most intriguing finding in EP models is the abrupt, first-order-like percolation transition. Although later studies confirmed that this transition is actually continuous [6–9], the intense scientific debate it sparked has significantly advanced percolation theory and network science [2–4]. Methods developed to verify the discontinuity of EP, such as gap scaling [10,11] and cluster-size heterogeneity [7], have been applied to characterize the critical behavior of various systems [12–17]. The mechanisms underlying explosive phenomena have also proven useful in network structure analysis [18–20] and immunization strategies [21].

Despite EP being widely recognized as a continuous phase transition, numerous studies have reported anomalous finite-size behaviors that deviate from standard finite-size scaling (FSS) theory [5,8,11,15,22,23]. A recent study introduced a dynamic ensemble called the event-based ensemble [24], where EP adheres to standard FSS theory. This approach explains the anomalous finite-size behaviors observed in

conventional ensembles with fixed bond density as a result of multiplex scalings induced by large fluctuations of the pseudocritical point, where clean FSS can be consistently observed.

The study of EP still faces unresolved issues and contradictions, particularly regarding the impact of intracluster bond insertion on critical phenomena. On one hand, inserting an intracluster bond, where both ends belong to the same cluster, does not directly affect cluster sizes but increases bond density, as depicted in Fig. 1. Thus, if potential bonds include intracluster ones, these might be preferentially inserted to curb cluster growth, aligning with the core mechanism of the Achlioptas process. On the other hand, adhering strictly to the product rule involves calculating size products without regard to whether the bond is intracluster, leading to a preference for inserting bonds between smaller clusters. These differences in bond insertion are illustrated in Fig. 1 by visually defining the size product P of an intracluster bond in a cluster of size s as $P = s^2$, $P = s$, or $P = 0$, which we refer to as square, linear, and zero rules, respectively.

In Fig. 2, we illustrate the FSS of the critical order parameter C_1/V for various competition rules of intracluster bonds, where C_1 is the size of the largest cluster and V is the total number of sites. It appears that linear and zero rules yield an asymptotic behavior of C_1/V for increasing V , which was interpreted as an indication of a discontinuous percolation transition [25]. Conversely, employing the product rule without differentiation between intracluster and intercluster bonds, i.e., square rule, results in a vanishing order parameter in an infinite system, akin to standard percolation.

Note that at criticality, the probability that a randomly chosen bond is an intracluster bond vanishes as the system volume V increases. This probability can be estimated as

$$V^{-1} \sum_{s=1}^{C_1} s^2 n(s, V) \sim V^{d_f(3-\tau)-1} \sim V^{-2(1-d_f)}. \quad (1)$$

*Contact author: lim@hfut.edu.cn

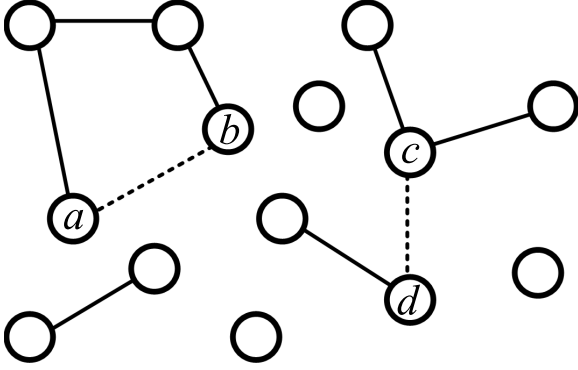


FIG. 1. A sketch of bond insertion rule in Achlioptas process, particularly for the differences between inter- and intracluster bonds. Here, circles, solid lines, and dashed lines represent sites, existing bonds, and potential bonds, respectively. A bond e_{ab} whose ends a and b are in the same cluster is called intracluster bond, while a bond e_{cd} whose ends c and d are in different clusters is called intercluster bond. The size s of a cluster is the number of sites in it. For sites a , b , c , and d , the sizes of corresponding clusters are $s_a = s_b = 4$, $s_c = 3$, and $s_d = 2$. For the intercluster bond e_{cd} , the size product is $P_{cd} = s_c \times s_d = 6$. For the intracluster bond e_{ab} , there are three typical definitions of the size product: $P_{ab} = s_a \times s_b = 16$, $P_{ab} = s_a = s_b = 4$, and $P_{ab} = 0$, which we refer to as square, linear, and zero rules, respectively. Consequently, e_{cd} is inserted when square rule is applied, and e_{ab} is inserted for linear and zero rules.

Here, $n(s, V)$ is the cluster number density, defined as the number of clusters with size s normalized by the system volume. Therefore, $s^2 n(s, V)/V$ represents the probability that two randomly chosen sites belong to the same cluster of

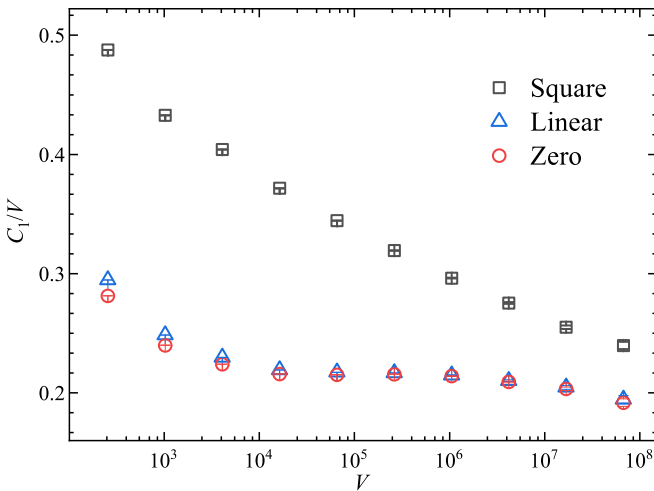


FIG. 2. The order parameter C_1/V at the infinite-volume critical point T_c is plotted as a function of the system volume V for EP under product rule. Here, C_1 represents the size of the largest cluster. For square rule, the order parameter C_1/V decreases as the system volume increases, and seems likely to vanish for infinite systems. Conversely, for linear and zero rules, where the insertion of intracluster bonds is prioritized, C_1/V appears to approach a constant value for infinite systems. In simulations, the critical point is set to $T_c = 0.8884491$ [24], which is defined as the total number of bonds at the percolation threshold normalized by the system volume.

size s . At criticality, the cluster number density scales as $n(s, V) \sim s^{-\tau}$, where τ is the Fisher exponent. In random graphs, where there is no concept of side length, the fractal dimension d_f is defined by the system volume relationship $C_1 \sim V^{d_f}$, known as the volume fractal dimension, and the hyperscaling relation reduces to $\tau = 1 + 1/d_f$, which is used in Eq. (1). Since $d_f < 1$, it is evident that the probability given by Eq. (1) vanishes for large V . This indicates that no intracluster bonds can be chosen as potential bonds in the infinite-volume limit, so that, the numerical results of Fig. 2, which are similarly presented in Ref. [25], cannot be used as effective evidence that systems of different competition mechanisms for intracluster bonds have different infinite-volume critical behaviors.

Furthermore, the insertion of intracluster bonds is crucial for the organization of high-order structures. A typical example of such structures is biconnected cluster (BC), where sites are connected by at least two independent paths. In standard percolation on random graphs, BC percolates at the same threshold as a connected cluster (CC) but exhibits different fractal dimensions [26,27]. Moreover, on low-dimensional hypercubic lattices [27–29] and complex networks [30–35], the nontrivial organization of high-order connectivity has unveiled significant geometric properties of percolation systems that cannot be captured by simple connections alone. For example, structures like the k core, consisting of compact clusters, can exhibit hybrid transitions involving both a jump of the giant cluster and a critical singularity at the percolation threshold [30,35–40]. Additionally, the critical behaviors of high-order structures of percolation clusters have also been demonstrated by the so-called backbones [41–44].

In this paper, our focus lies on exploring the high-order organization of critical clusters in EP. We reveal that EP of different competition rules for intracluster bonds share the same percolation threshold and universality, while the fractal dimension of BCs is rule dependent. Additionally, the cluster number density of BCs shows a double-scaling behavior, also depending on the competition rule of intracluster bonds.

The remainder of this paper is organized as follows. Section II shows the details of the model, algorithm, and observables. In Sec. III, we show the simulation results of the EP under three competition rules of intracluster bonds. The FSS behaviors of BCs are studied in Sec. IV. We include a short discussion in the final section.

II. MODEL, ALGORITHM, AND OBSERVABLES

The Achlioptas process initiates with a null graph of volume V , then proceeds by inserting bonds step by step. At each time step, two potential bonds, denoted as e_{ab} and e_{cd} , are randomly selected from all unconnected pairs of sites. Here, a , b , c , and d denote the sites. Subsequently, the size products $P_{ab} = s_a \times s_b$ and $P_{cd} = s_c \times s_d$ are computed, where s_i denotes the size of the cluster that site i belongs to. If $P_{ab} < P_{cd}$, bond e_{ab} is inserted, and bond e_{cd} is discarded. In the case of $P_{ab} = P_{cd}$, one bond is randomly chosen for insertion. This mechanism defines the product rule of EP [1].

For intracluster bonds, sites at the two ends belong to the same cluster (see Fig. 1), thus, a specialized definition for the size product P is necessary. Generally, three approaches

are considered: $P = s^2$, $P = s$, and $P = 0$, where s represents the size of the cluster to which the intracluster bond belongs. For convenience, we refer to them as square, linear, and zero rules, respectively. In zero rule ($P = 0$), intracluster bonds are prioritized for insertion, leading to the system tending to form large dense clusters. Conversely, with square rule ($P = s^2$), intracluster bonds are hardly inserted into large clusters, due to their significantly larger size product. The linear rule ($P = s$) represents an intermediate scenario between these two scenarios.

To apply the event-based ensemble effectively, we need to define a dynamic pseudocritical point for each individual realization, where all quantities are sampled and averaged. We propose two such critical points based on the sizes of the largest CC and BC, respectively. In each run of the Achlioptas process, we monitor the size of the largest CC, denoted as $\mathcal{C}_1(t)$, at each time step t . Then, we calculate the one-step incremental size of the largest CC as $\Delta(t) = \mathcal{C}_1(t+1) - \mathcal{C}_1(t)$. The dynamic pseudocritical point \mathcal{T}_V for a single realization is defined as $\mathcal{T}_V = t_{\max}/V$, where t_{\max} represents the time step at which $\Delta(t)$ reaches its maximum value. Similarly, another dynamic pseudocritical point \mathcal{T}'_V can be defined based on the one-step incremental size of the largest BC, denoted as $\Delta'(t) = \mathcal{B}_1(t+1) - \mathcal{B}_1(t)$, where \mathcal{B}_1 represents the size of the largest BC.

In our simulations, we employ the Newman-Ziff algorithm to track the growth of \mathcal{C}_1 during the bond-insertion process [45], as it allows for real-time updates of evolving clusters using a data structure known as disjoint set [46]. However, it is worth noting that a site can belong to multiple BCs simultaneously. Therefore, the Newman-Ziff algorithm, which relies on disjoint sets, is not suitable for storing information about BCs. To maintain dynamic BCs, we employ a data structure, called block forest [47]. The block tree is constructed by identifying blocks (BCs) and their articulation points, resulting in a tree structure where each node represents either a BC or an articulation point. An articulation point is a site whose removal increases the number of CCs in the graph, and edges in this tree represent the inclusion of articulation points within these BCs. When a newly inserted bond bridges two nodes (BCs or articulation points), the block tree is updated by condensing a chain of nodes between the two nodes into a new node (BC). This dynamic update allows for real-time recording of BC information. Hence, this data structure can be readily adapted to the EP model, enabling real-time tracking of the one-step incremental size of the largest BC.

In each realization of EP, we first identify the pseudocritical points \mathcal{T}_V and \mathcal{T}'_V , then at the two dynamic pseudocritical points, we sample and calculate the following observables:

(1) The mean pseudocritical point $\mathcal{T}_V \equiv \langle \mathcal{T}_V \rangle$ and $\mathcal{T}'_V \equiv \langle \mathcal{T}'_V \rangle$, and their fluctuations $\sigma(\mathcal{T}_V) \equiv \sqrt{\langle \mathcal{T}_V^2 \rangle - \langle \mathcal{T}_V \rangle^2}$ and $\sigma(\mathcal{T}'_V) \equiv \sqrt{\langle \mathcal{T}'_V{}^2 \rangle - \langle \mathcal{T}'_V \rangle^2}$.

(2) The size of the n th largest CC, $\mathcal{C}_n \equiv \langle \mathcal{C}_n \rangle$, and the size of the n th largest BC, $\mathcal{B}_n \equiv \langle \mathcal{B}_n \rangle$, where \mathcal{C}_n and \mathcal{B}_n refer to the values in a single realization.

(3) The cluster number density of BCs, $n(s, V) \equiv \langle \mathcal{N}_s \rangle / V$, where \mathcal{N}_s is the number of BCs with size s in a single realization.

Here, the brackets $\langle \cdot \rangle$ denote the average of different realizations in the event-based ensemble.

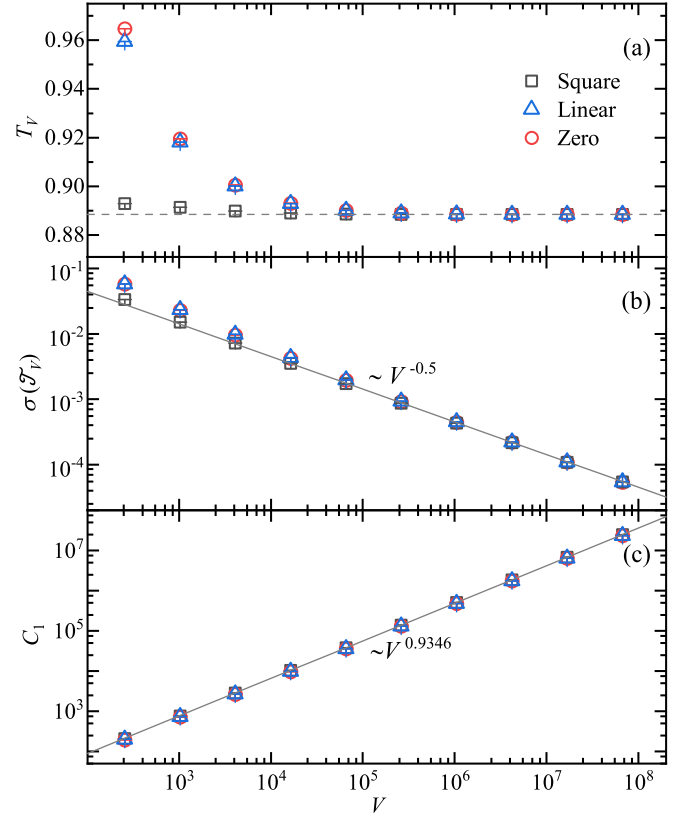


FIG. 3. The FSS of EP for different competition rules of intracluster bonds. (a) The asymptotic behavior of the pseudocritical point \mathcal{T}_V versus system volume V . Although for finite V , the three scenarios show different pseudocritical points \mathcal{T}_V , they are convergent to the same value $T_c \approx 0.888449$ for large systems indicated by the dashed line. The fit results for these asymptotic behaviors are listed in Table I. (b) The plots of the dynamic pseudocritical point fluctuation $\sigma(\mathcal{T}_V)$ versus system volume V . The fit results in Table I suggest that all three scenarios have the same FSS $\sigma \sim V^{-1/2}$ indicated by the solid line. (c) The size of the largest CC sampled at the dynamic pseudocritical point, $\mathcal{C}_1 \equiv \langle \mathcal{C}_1 \rangle$, as a function of system volume V . The solid line represents the fit result $d_f = 0.9346$ in Table I.

III. PERCOLATION OF CONNECTED CLUSTERS

In this section, we study the percolation of CCs under different competition rules of intracluster bonds. The data shown in this section is extracted at the dynamic pseudocritical point \mathcal{T}_V identified by the largest one-step incremental size of the largest CC.

In Fig. 3(a), we observe the asymptotic behavior of the pseudocritical point \mathcal{T}_V plotted against the system volume V . For zero rule, the system exhibits the largest pseudocritical point among the three scenarios, due to the preferential insertion of intracluster bonds, which decays the onset of percolation. Conversely, EP under square rule demonstrates the smallest pseudocritical point due to its blind bond insertion approach, where intracluster bonds are not given special preference. Nevertheless, with the increasing of system volumes, these pseudocritical points approach the same value, as indicated by the dashed line in Fig. 3(a).

TABLE I. The fit results of the infinite-volume critical point T_c , the reciprocal value of the correlation-length exponent $1/\nu$, the exponent θ to describe the fluctuation of \mathcal{T}_V , and the fractal dimension d_f of the largest CC for different competition rules of intracluster bonds. Here, the data are all sampled at the dynamic pseudocritical point \mathcal{T}_V , where the one-step increment size of \mathcal{C}_1 reaches its maximum value. Within error bars, the three scenarios suggest the same percolation threshold, and critical exponents.

Rule	T_c	$1/\nu$	θ	d_f
Square	0.888 449 3(3)	0.74(5)	0.499(1)	0.9346(2)
Linear	0.888 449 3(4)	0.741(6)	0.495(5)	0.9347(1)
Zero	0.888 449 0(2)	0.741(1)	0.49(2)	0.9346(3)

To quantify these asymptotic behaviors, we fit the Monte Carlo data of \mathcal{T}_V to the FSS ansatz

$$\mathcal{T}_V = T_c + V^{-1/\nu}(a_0 + a_1 V^{-\omega} + \dots). \quad (2)$$

Here, T_c denotes the infinite-volume critical point, ν is the critical exponent of the correlation length, and the term $V^{-\omega}$ is a correction to the FSS. If the correction term is excluded, i.e., ($a_1 = 0$), the fitting results are sensitive to the changes of the lower cutoff V_{\min} on the data points admitted in the fit. With all the terms of the FSS ansatz Eq. (2) free, we estimate the stable fit for T_c and $1/\nu$ as listed in Table I. Choosing the optimal fit for the FSS ansatz typically involves identifying the smallest value of V_{\min} for which the χ^2 per degree of freedom is close to unity. Specifically, χ^2 is calculated as the sum of the squared differences between observed values and the fitting curve, each normalized by the errors of observations. Moreover, further increases in V_{\min} should not result in significant reductions in the χ^2 value beyond one unit per degree of freedom.

The results presented in Table I demonstrate that, within the error margins, the pseudocritical points for all three scenarios converge to the same percolation threshold, $T_c = 0.888\,449$, aligning with the percolation threshold of EP reported in the previous studies [7,24]. It indicates that the percolation threshold in EP remains consistent regardless of competition rules governing the insertion of intracluster bonds. Furthermore, the critical exponent ν is also consistent across all three scenarios within the error margins, suggesting that the percolation transitions of CCs for different competition rules of intracluster bonds belong to the same universality class. It is worth noting that simulations in the conventional ensemble of fixed bond densities might erroneously suggest variations in percolation thresholds among different rules [25].

Further, we can estimate the volume fractal dimension d_f from the observable \mathcal{C}_1 sampled at the dynamic pseudocritical point, by fitting the data to the FSS ansatz

$$\mathcal{C}_1 = V^{d_f}(a_0 + a_1 V^{-\omega_1} + a_2 V^{-\omega_2} + \dots), \quad (3)$$

where ω_i ($i = 1, 2$) denotes the correction exponents. The stable fit can be obtained by including only one correction term ($a_2 = 0$) in Eq. (3), and the results are listed in Table I. The consistency of the fractal dimension across all three scenarios further emphasizes the independence of the EP nature from the competition rule of intracluster bonds, which is visually

TABLE II. The fit results of the infinite-volume critical point T_c , the reciprocal value of the correlation-length exponent $1/\nu$, the exponent θ to describe the fluctuation of \mathcal{T}'_V , and the fractal dimension d'_f of the largest BC for different competition rules of intracluster bonds. Here, the data are all sampled at the dynamic pseudocritical point \mathcal{T}'_V , where the one-step increment size of \mathcal{B}_1 reaches its maximum value. Within error bars, T_c , $1/\nu$, and θ take the same value as those obtained by CC (Table I), which is independent of the competition rules of intracluster bonds. However, the fractal dimension d'_f varies across different rules.

Rule	T_c	$1/\nu$	θ	d_f	d'_f
Square	0.888 449 4(3)	0.74(2)	0.49(2)	0.9347(2)	0.511(1)
Linear	0.888 449 3(5)	0.74(1)	0.50(9)	0.9363(5)	0.560(5)
Zero	0.888 449 0(4)	0.74(1)	0.4(2)	0.9367(8)	0.575(8)

displayed by the nearly complete overlap of the FSS of \mathcal{C}_1 for the three scenarios, as depicted in Fig. 3(c).

The discrepancy between the finite-size behaviors observed at the dynamic pseudocritical point \mathcal{T}_V and the infinite-volume critical point T_c , as depicted in Figs. 2 and 3, highlights an intriguing aspect of the EP dynamics. This contrast is further elucidated by studying the fluctuation $\sigma(\mathcal{T}_V)$ as a function of system volume V [24], as shown in Fig. 3(b). The well-defined scaling behavior $\sigma(\mathcal{T}_V) \sim V^{-\theta}$, where $\theta < 1/\nu$, indicates that the pseudocritical point of EP can deviate significantly from T_c in some realizations, leading to distinct finite-size behaviors at \mathcal{T}_V compared to T_c .

Moreover, it is proposed that the scaling window is effectively defined around \mathcal{T}_V rather than T_c [24]. Consequently, the FSS extracted at T_c encompasses a mixture of behaviors observed over a wide range of bond densities, potentially spanning both super- and subcritical phases. This mixture effect under different competition rules of intracluster bonds gives rise to the anomalous finite-size behaviors depicted in Fig. 2, highlighting the nuanced nature of the EP dynamics.

To determine the value of θ , we fit the data of $\sigma(\mathcal{T}_V)$ to the scaling ansatz Eq. (3), where the exponent d_f is replaced by $-\theta$. Including one correction term, the stable fit results suggest a consistent exponent $\theta = 1/2$ for various competition rules of intracluster bonds (Table I). This finding supports the argument that the distribution of \mathcal{T}_V in EP follows the central limit theorem and obeys a normal distribution [24,48], which could be a universal property for EP of various rules.

IV. PERCOLATION OF BICONNECTED CLUSTERS

In this section, we study the percolation transition of BCs in EP under different competition rules of intracluster bonds. The data shown in this section is extracted at the dynamic pseudocritical point \mathcal{T}'_V identified by the largest one-step increment size of the largest BC.

A. Asymptotic behavior of the pseudocritical point \mathcal{T}'_V

In Fig. 4(a), we plot the pseudocritical point \mathcal{T}'_V versus the system volume V . It is evident that \mathcal{T}'_V varies for different competition rules of intracluster bonds. Because BCs are always

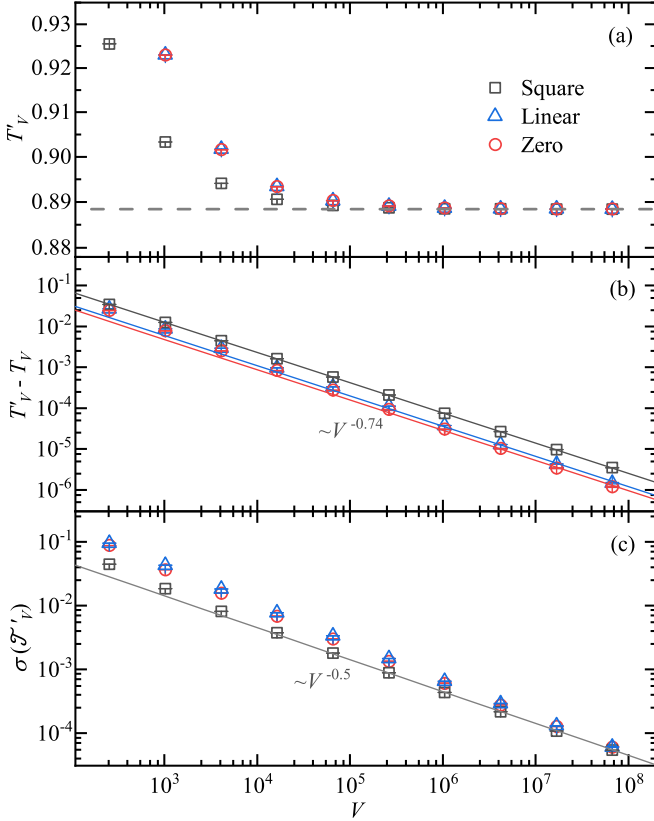


FIG. 4. The asymptotic behaviors of the pseudocritical point T'_V identified by the one-step incremental size of the largest BC for different competition rules of intracluster bonds. (a) The pseudocritical point T'_V is plotted as a function of system volume V . Although for finite V , the three scenarios show different pseudocritical points T'_V , they are convergent to the same percolation threshold $T'_V = 0.888449$ for large systems, which is consistent with the percolation threshold of CCs. The fit results for these asymptotic behaviors are shown in Table II. (b) The distance between the pseudocritical points T_V and T'_V for different competition rules of intracluster bonds. All three lines represent the power-law decay with exponent 0.74, which is just the reciprocal value of the correlation-length exponent $1/\nu$ listed in Tables I and II. (c) The plots of the fluctuation of the dynamic pseudocritical point $\sigma(T'_V)$ versus system volume V , indicating that all the three scenarios have the same scaling $\sigma \sim V^{-1/2}$.

formed out of CCs, a system with a large T_V also has a large T'_V , as depicted in Fig. 4(a).

To capture the asymptotic behavior of the pseudocritical point T'_V , we conduct a least-square fit to the Monte Carlo data of T'_V using the scaling ansatz Eq. (2). Accounting for systematic errors, we obtain estimates summarized in Table II. The fit results reveal that the infinite-volume critical point coincides with the percolation threshold of CCs (Table I), indicating that CCs and BCs percolate simultaneously in EP, irrespective of the competition rule of intracluster bonds.

Furthermore, within the margin of errors, the fit results in Table II suggest identical exponents $1/\nu$ and θ as those for T_V . This implies that the pseudocritical points identified by CCs and BCs exhibit the same asymptotic behavior, corroborated by the power-law decay of $T'_V - T_V \sim V^{-1/\nu}$ depicted in Fig. 4(b). The scaling behavior of the fluctuation

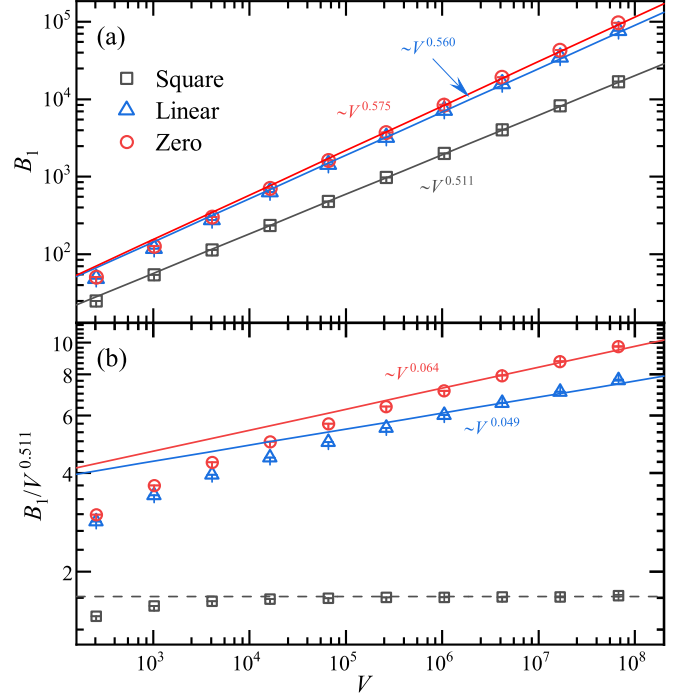


FIG. 5. The FSS of the size of the largest BC sampled at the dynamic pseudocritical point T'_V for different competition rules of intracluster bonds. (a) The size B_1 of the largest BC as a function of system volume V . The fit results of Table II are indicated by lines. (b) The ratio $B_1/V^{0.511}$ as a function of system volume V . For square rule, the fractal dimension is $d'_f = 0.511$, thus, the ratio $B_1/V^{0.511}$ approaches a constant for large V , indicated by the dashed line. For the other two rules, the ratio $B_1/V^{0.511}$ shows a power-law growth for large V , and the exponent of the power-law growth is consistent with the fit result in Table II. This suggests that the critical BC has different fractal dimensions under different competition rules of intracluster bonds.

$\sigma(T'_V) \sim V^{-\theta}$ with $\theta = 1/2$ is also evident in Fig. 4(c). Importantly, these scalings are independent of the competition rule of intracluster bonds, which solely influences finite-size corrections.

B. Fractal dimension of biconnected clusters

In Fig. 5(a), we observe the power-law growth of the size B_1 of the largest BC sampled at the dynamic pseudocritical point T'_V for different competition rules of intracluster bonds. This growth behavior signifies the fractal nature of the critical BC, with the fractal dimension d'_f being dependent on the competition rule of intracluster bonds.

To quantify the fractal dimension d'_f of the critical BC, we perform fits to the FSS ansatz Eq. (3) and summarize the estimates in Table II. The differences between the d'_f values obtained in different scenarios are significant, compared to the error bars, confirming distinct fractal dimensions of BCs. For better visualization of these differences, we plot the ratio $B_1/V^{0.511}$ for all three scenarios in Fig. 5(b). Notably, for square rule, where the fractal dimension is $d'_f = 0.511$, the ratio $B_1/V^{0.511}$ tends to approach a constant for large V . However, for the other two rules, this ratio exhibits a power-law

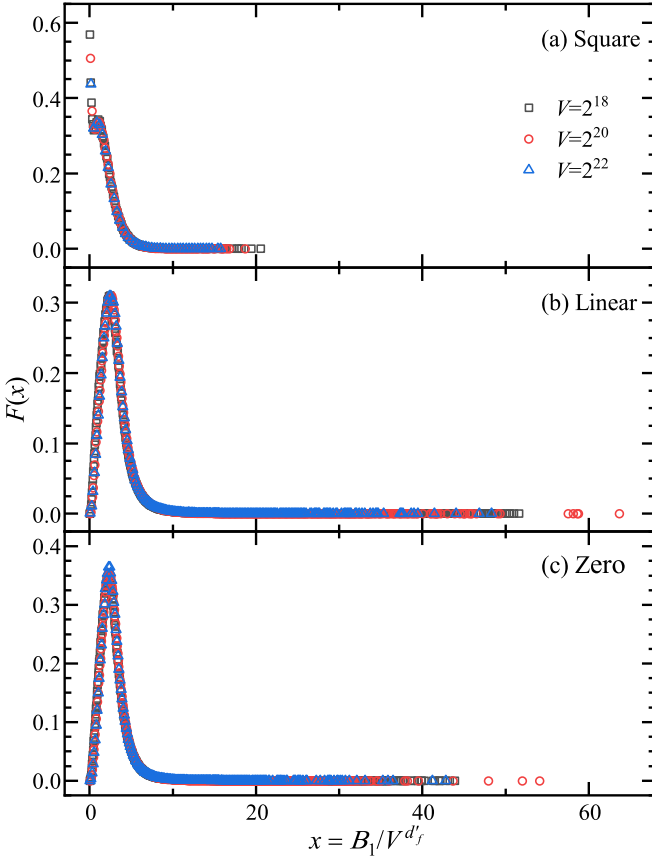


FIG. 6. The probability distribution $F(x)$ of the size of the largest BC sampled at the dynamic pseudocritical point \mathcal{T}'_V for (a) square, (b) linear, and (c) zero rules. By defining $x \equiv B_1/V^{d'_f}$ with the fit result of d'_f in Table II, all the three scenarios show nice collapses of data from different system volumes, confirming the unique d'_f for each scenario.

growth for large V , indicating different fractal dimensions of BCs.

For comparison, we also sample the size C_1 of the largest CC at the dynamic pseudocritical point \mathcal{T}'_V . The fit results for d_f are listed in Table II, and within double error bars, these values are identical. This indicates that the fractal dimension d_f of the critical CC at \mathcal{T}'_V is independent of the competition rule of intracluster bonds and has the same value as the one sampled at \mathcal{T}_V (Table I). This consistency arises naturally as \mathcal{T}_V and \mathcal{T}'_V exhibit the same asymptotic behavior and is both situated within the scaling window $\mathcal{O}(V^{-1/\nu})$.

To further confirm the unique fractal dimension of the critical BC, we examine the probability distribution $F(x)$ of the size of the largest BC in Fig. 6. By defining $x \equiv B_1/V^{d'_f}$ using the fit result of d'_f from Table II, we achieve a well-renormalized distribution, demonstrating a collapse of data from different system volumes for all three scenarios. This validates the distinct fractal dimensions d'_f for different competition rules of intracluster bonds.

C. Cluster number density

By utilizing the hyperscaling relation $\tau' = 1 + 1/d'_f > 2$ along with the fractal dimension d'_f listed in Table II,

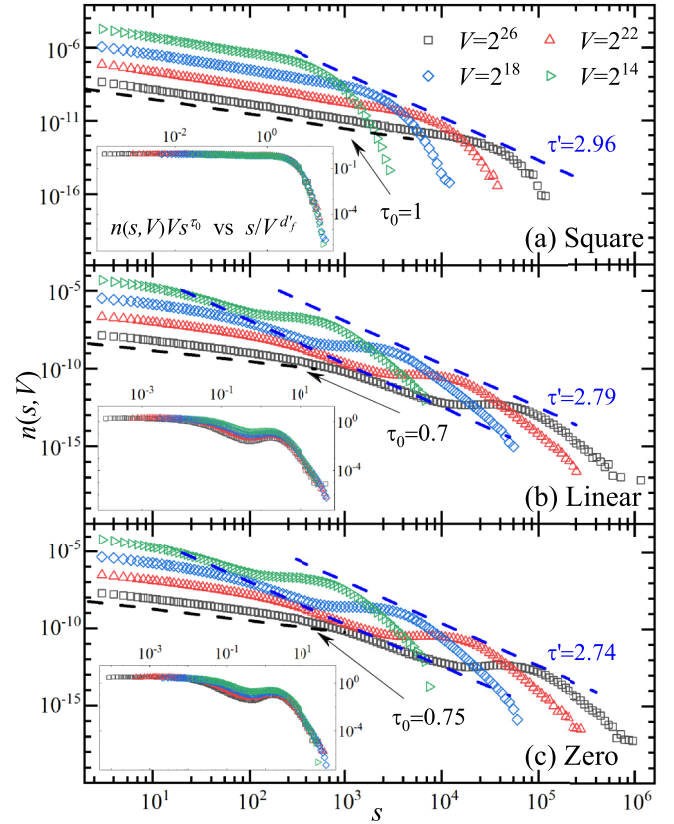


FIG. 7. The cluster number density of BCs for different competition rules of intracluster bonds. (a) Square rule. (b) Linear rule. (c) Zero rule. Two scalings can be observed for finite BCs, separated by a characteristic size s_0 . The standard Fisher exponent $\tau' = 1 + 1/d'_f$ dominates the size distribution for $s \gg s_0$, while the size distribution for $s \ll s_0$ shows a modified Fisher exponent τ_0 . The part $s < s_0$ decreases as a whole for increasing system volume V . The insets show the rescaled cluster number density of BCs $n(s, V)V s^{\tau_0}$ as a function of $s/V^{d'_f}$, where the fit results of d'_f in Table II are used. The nice data collapse for $s < s_0$ suggests that $n(s, V) \sim V^{-1}$ for all the three scenarios. In addition, the plots also suggest $\tau_0 \approx 1, 0.7, \text{ and } 0.75$ for the three scenarios, respectively.

we can immediately determine the Fisher exponent τ' for BCs. However, the size distribution of BCs cannot be fully characterized by this standard Fisher exponent, instead, it exhibits a double-scaling behavior, as depicted in Fig. 7. Specifically, for linear and zero rules [Figs. 7(b) and 7(c)], apart from the standard characteristic size $s_\xi \sim V^{d'_f}$, another characteristic size s_0 emerges, which also grows as the system volume increases. For $s \ll s_0$, a modified Fisher exponent $\tau_0 < \tau'$ is observed, while for $s \gg s_0$, the size distribution of BCs is predominantly governed by the standard Fisher exponent τ' , rapidly decaying for $s > s_\xi$. Moreover, the overall cluster number density $n(s, V)$ for $s < s_0$ decreases with increasing system volume V . From this viewpoint of double scaling, systems of square rule correspond to an s_0 that is equal to or slightly smaller than s_ξ , resulting in a seemingly pure power-law distribution governed only by τ_0 , see Fig. 7(a).

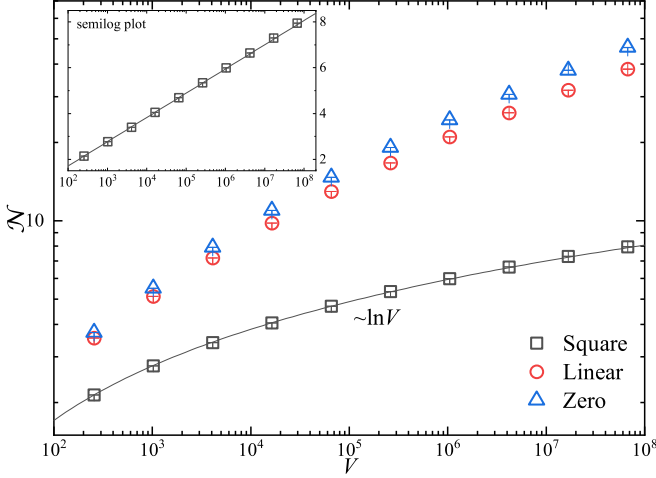


FIG. 8. The total number of BCs \mathcal{N} at the dynamic pseudocritical point \mathcal{T}_V for different competition rules of intracluster bonds. For square rule, \mathcal{N} presents a logarithmic growth with increasing system volume V . The line shows the function of $\mathcal{N} \sim \ln V$. The straight line of the same data in the semilog plot also confirms the logarithmic growth of \mathcal{N} , see the inset. For linear and zero rules, the growth of \mathcal{N} can neither be fitted by a power law function nor a logarithmic function, which would have some intricate finite-size corrections that are not represented by the used fit function.

From these observations, we propose an expression for the cluster number density $n(s, V)$ of BCs as follows:

$$n(s, V) = \begin{cases} As^{-\tau_0}, & s \ll s_0, \\ s^{-\tau'} \tilde{n}(s/s_\xi), & s \gg s_0, \end{cases} \quad (4)$$

where A is a V -dependent parameter ensuring the normalizability of the cluster size distribution $sn(s, V)$ for $\tau_0 \leq 2$. The normalizing condition $A \int_1^{s_0} s^{1-\tau_0} ds + \int_{s_0}^{s_\xi} s^{1-\tau'} ds \sim \mathcal{O}(1)$ yields $A \leq \mathcal{O}(s_0^{\tau_0-2})$, where $\tau_0 < 2$ and $\tau' > 2$ from the observation in Fig. 7. The insets of Fig. 7 demonstrate $n(s, V)V s^{\tau_0}$ as a function of s/V^{d_f} , with data from various system volumes collapsing well. This collapse indicates $A \sim V^{-1}$ for all three scenarios, regardless of τ_0 . It is worth noting that for standard percolation on random graphs, $n(s, V) \sim V^{-1}$ for BCs as well [27,49].

To further understand the different $n(s, V)$ of the three scenarios in Fig. 7, we study the FSS of the total number of BCs, calculated as $\mathcal{N} = V \sum_{s=1}^{s_0} n(s, V)$. Calling Eq. (4), the total number of BCs can be estimated as

$$\mathcal{N} \sim AV \int_1^{s_0} s^{-\tau_0} ds + V \int_{s_0}^{s_\xi} s^{-\tau'} ds. \quad (5)$$

The FSS behavior of \mathcal{N} is dependent on s_0 and τ_0 . If s_0 is absent, Eq. (5) yields $\mathcal{N} \sim V$, which corresponds to the observation for CCs. However, the simulation results in Fig. 8 clearly demonstrate that for all three scenarios, \mathcal{N} of BCs diverges slower than $\sim V$, suggesting a nontrivial s_0 . For square rule, the total number of BCs is well described by the logarithmic function, i.e., $\mathcal{N} \sim \ln V$. To account for this

behavior using Eq. (5), it requires $\tau_0 = 1$ in the first term, and $s_0 \sim s_\xi$ in the second term. This explains the scaling behavior in Fig. 7(a), where all finite BCs exhibit a size distribution with $\tau_0 = 1$.

The data collapse in the insets of Figs. 7(b) and 7(c) suggest $\tau_0 \approx 0.7$ and 0.75 for linear and zero rules, respectively. For these $\tau_0 < 1$, both terms in Eq. (5) diverge as $s_0 \rightarrow \infty$ for $V \rightarrow \infty$, and the leading behavior depends on the FSS behavior of s_0 . Due to the lack of direct measurement for s_0 , its FSS is unavailable in our phenomenological discussion. From Fig. 8, where the divergence of \mathcal{N} for linear and zero rules cannot be captured by a simple logarithmic or power-law function, it is suggested that the FSS of s_0 should include strong finite-size corrections.

From the preceding discussion, we ascertain that the modified Fisher exponent τ_0 stems from the vanishing cluster number density $n(s, V)$ for $s < s_0$. Such vanishing cluster number density phenomena have also been observed for leaf-free and bridge-free clusters in high-dimensional percolation [27] and holes in no-enclave percolation [50]. Here, the cluster number density of BCs might exhibit a more intricate behavior, contingent upon the competition rule of intracluster bonds.

V. CONCLUSION

In this study, we delve into the percolation transition of high-order connectivity in EP through three specific competition rules of intracluster bonds in the Achlioptas process. Extensive simulations corroborate that EP, regardless of competition rules applied to intracluster bonds, conforms to the same percolation threshold and universality class. This clarifies that the competition rules of intracluster bonds do not affect the critical behaviors of EP. However, the finite-size behaviors of BCs are very sensitive to these rules, and we provide strong numerical evidence demonstrating the rule-dependent fractal dimensions of BCs. Additionally, BCs exhibit unique properties, such as a double-scaling behavior in size distribution, requiring a modified Fisher exponent to describe the size distribution of small BCs.

Our findings contribute to resolving the debate regarding the universality of EP in relation to the competition rules of intracluster bonds, and demonstrate the superiority of the event-based ensemble over the conventional fixed bond density ensemble in accurately extracting the FSS behavior. Building on these findings, we reveal the presence of nontrivial high-order connectivity within percolation clusters, despite EP focusing solely on simply connected clusters. Therefore, it would be intriguing to explore the emergence of other high-order connectivities in EP and investigate the potential existence of a genuine discontinuous transition within the Achlioptas process.

ACKNOWLEDGMENTS

The authors acknowledge helpful discussions with S. Fang. The research was supported by the Fundamental Research Funds for the Central Universities (No. JZ2023HGTB0220).

- [1] D. Achlioptas, R. M. D'Souza, and J. Spencer, Explosive percolation in random networks, *Science* **323**, 1453 (2009).
- [2] S. Boccaletti, J. Almendral, S. Guan, I. Leyva, Z. Liu, I. Sendiña-Nadal, Z. Wang, and Y. Zou, Explosive transitions in complex networks' structure and dynamics: Percolation and synchronization, *Phys. Rep.* **660**, 1 (2016).
- [3] R. M. D'Souza, J. Gómez-Gardeñes, J. Nagler, and A. Arenas, Explosive phenomena in complex networks, *Adv. Phys.* **68**, 123 (2019).
- [4] M. Li, R.-R. Liu, L. Lü, M.-B. Hu, S. Xu, and Y.-C. Zhang, Percolation on complex networks: Theory and application, *Phys. Rep.* **907**, 1 (2021).
- [5] E. J. Friedman and A. S. Landsberg, Construction and analysis of random networks with explosive percolation, *Phys. Rev. Lett.* **103**, 255701 (2009).
- [6] R. A. da Costa, S. N. Dorogovtsev, A. V. Goltsev, and J. F. F. Mendes, Explosive percolation transition is actually continuous, *Phys. Rev. Lett.* **105**, 255701 (2010).
- [7] H. K. Lee, B. J. Kim, and H. Park, Continuity of the explosive percolation transition, *Phys. Rev. E* **84**, 020101(R) (2011).
- [8] P. Grassberger, C. Christensen, G. Bizhani, S.-W. Son, and M. Paczuski, Explosive percolation is continuous, but with unusual finite size behavior, *Phys. Rev. Lett.* **106**, 225701 (2011).
- [9] O. Riordan and L. Warnke, Explosive percolation is continuous, *Science* **333**, 322 (2011).
- [10] S. Manna and A. Chatterjee, A new route to explosive percolation, *Physica A* **390**, 177 (2011).
- [11] J. Nagler, A. Levina, and M. Timme, Impact of single links in competitive percolation, *Nature Phys.* **7**, 265 (2011).
- [12] J. D. Noh, H. K. Lee, and H. Park, Scaling of cluster heterogeneity in percolation transitions, *Phys. Rev. E* **84**, 010101(R) (2011).
- [13] J.-P. Lv, X. Yang, and Y. Deng, Scaling of cluster heterogeneity in the two-dimensional Potts model, *Phys. Rev. E* **86**, 022105 (2012).
- [14] W. S. Jo, S. D. Yi, S. K. Baek, and B. J. Kim, Cluster-size heterogeneity in the two-dimensional Ising model, *Phys. Rev. E* **86**, 032103 (2012).
- [15] J. Fan, J. Meng, Y. Liu, A. A. Saberi, J. Kurths, and J. Nagler, Universal gap scaling in percolation, *Nature Phys.* **16**, 455 (2020).
- [16] M. Feshanjerdi and A. A. Saberi, Universality class of epidemic percolation transitions driven by random walks, *Phys. Rev. E* **104**, 064125 (2021).
- [17] M. Feshanjerdi, A. A. Masoudi, P. Grassberger, and M. Ebrahimi, Aftermath epidemics: Percolation on the sites visited by generalized random walks, *Phys. Rev. E* **108**, 024312 (2023).
- [18] R. K. Pan, M. Kivelä, J. Saramäki, K. Kaski, and J. Kertész, Using explosive percolation in analysis of real-world networks, *Phys. Rev. E* **83**, 046112 (2011).
- [19] M. Schröder, J. Nagler, M. Timme, and D. Witthaut, Hysteretic percolation from locally optimal individual decisions, *Phys. Rev. Lett.* **120**, 248302 (2018).
- [20] Z. Qiu, T. Fan, M. Li, and L. Lü, Identifying vital nodes by Achlioptas process, *New J. Phys.* **23**, 033036 (2021).
- [21] P. Clusella, P. Grassberger, F. J. Pérez-Reche, and A. Politi, Immunization and targeted destruction of networks using explosive percolation, *Phys. Rev. Lett.* **117**, 208301 (2016).
- [22] H. Hooyberghs and B. V. Schaebroeck, Criterion for explosive percolation transitions on complex networks, *Phys. Rev. E* **83**, 032101 (2011).
- [23] R. M. D'Souza and J. Nagler, Anomalous critical and supercritical phenomena in explosive percolation, *Nature Phys.* **11**, 531 (2015).
- [24] M. Li, J. Wang, and Y. Deng, Explosive percolation obeys standard finite-size scaling in an event-based ensemble, *Phys. Rev. Lett.* **130**, 147101 (2023).
- [25] Y. S. Cho and B. Kahng, Suppression effect on explosive percolation, *Phys. Rev. Lett.* **107**, 275703 (2011).
- [26] M. E. J. Newman and G. Ghoshal, Bicomponents and the robustness of networks to failure, *Phys. Rev. Lett.* **100**, 138701 (2008).
- [27] W. Huang, P. Hou, J. Wang, R. M. Ziff, and Y. Deng, Critical percolation clusters in seven dimensions and on a complete graph, *Phys. Rev. E* **97**, 022107 (2018).
- [28] X. Xu, J. Wang, Z. Zhou, T. M. Garoni, and Y. Deng, Geometric structure of percolation clusters, *Phys. Rev. E* **89**, 012120 (2014).
- [29] Z. Zhou, X. Xu, T. M. Garoni, and Y. Deng, Leaf-excluded percolation in two and three dimensions, *Phys. Rev. E* **91**, 022140 (2015).
- [30] D. Cellai, A. Lawlor, K. A. Dawson, and J. P. Gleeson, Tricritical point in heterogeneous k -core percolation, *Phys. Rev. Lett.* **107**, 175703 (2011).
- [31] Y.-Y. Liu, E. Csóka, H. Zhou, and M. Pósfai, Core percolation on complex networks, *Phys. Rev. Lett.* **109**, 205703 (2012).
- [32] M. Li, Y. Deng, and B.-H. Wang, Clique percolation in random graphs, *Phys. Rev. E* **92**, 042116 (2015).
- [33] A. R. Benson, D. F. Gleich, and J. Leskovec, Higher-order organization of complex networks, *Science* **353**, 163 (2016).
- [34] L. Tian, A. Bashan, D.-N. Shi, and Y.-Y. Liu, Articulation points in complex networks, *Nat. Commun.* **8**, 14223 (2017).
- [35] S. Osat, F. Radicchi, and F. Papadopoulos, k -core structure of real multiplex networks, *Phys. Rev. Res.* **2**, 023176 (2020).
- [36] A. V. Goltsev, S. N. Dorogovtsev, and J. F. F. Mendes, k -core (bootstrap) percolation on complex networks: Critical phenomena and nonlocal effects, *Phys. Rev. E* **73**, 056101 (2006).
- [37] S. Gao, L. Xue, B. Gross, Z. She, D. Li, and S. Havlin, Possible origin for the similar phase transitions in k -core and interdependent networks, *New J. Phys.* **26**, 013006 (2024).
- [38] Y. Shang, Attack robustness and stability of generalized k -cores, *New J. Phys.* **21**, 093013 (2019).
- [39] Y. Shang, Generalized k -core percolation in networks with community structure, *SIAM J. Appl. Math.* **80**, 1272 (2020).
- [40] Y. Shang, Generalized k -core percolation on correlated and uncorrelated multiplex networks, *Phys. Rev. E* **101**, 042306 (2020).
- [41] Y. Gefen, A. Aharony, B. B. Mandelbrot, and S. Kirkpatrick, Solvable fractal family, and its possible relation to the backbone at percolation, *Phys. Rev. Lett.* **47**, 1771 (1981).
- [42] M. Porto, A. Bunde, S. Havlin, and H. E. Roman, Structural and dynamical properties of the percolation backbone in two and three dimensions, *Phys. Rev. E* **56**, 1667 (1997).

- [43] M. Barthélemy, S. V. Buldyrev, S. Havlin, and H. E. Stanley, Scaling for the critical percolation backbone, *Phys. Rev. E* **60**, R1123(R) (1999).
- [44] S. Fang, D. Ke, W. Zhong, and Y. Deng, Backbone and shortest-path exponents of the two-dimensional q -state Potts model, *Phys. Rev. E* **105**, 044122 (2022).
- [45] M. E. J. Newman and R. M. Ziff, Efficient Monte Carlo algorithm and high-precision results for percolation, *Phys. Rev. Lett.* **85**, 4104 (2000).
- [46] Z. Galil and G. F. Italiano, Data structures and algorithms for disjoint set union problems, *ACM Comput. Surv.* **23**, 319 (1991).
- [47] J. Westbrook and R. E. Tarjan, Maintaining bridge-connected and biconnected components on-line, *Algorithmica* **7**, 433 (1992).
- [48] M. Feshanjerdi and P. Grassberger, Extreme-value statistics and super-universality in critical percolation? [arXiv:2401.05234](https://arxiv.org/abs/2401.05234).
- [49] E. Ben-Naim and P. L. Krapivsky, Kinetic theory of random graphs: From paths to cycles, *Phys. Rev. E* **71**, 026129 (2005).
- [50] H. Hu, R. M. Ziff, and Y. Deng, No-enclave percolation corresponds to holes in the cluster backbone, *Phys. Rev. Lett.* **117**, 185701 (2016).